Actuator Cylinder Theory for Multiple Vertical Axis Wind Turbines

Andrew Ning

Brigham Young University, Provo, UT, USA

Correspondence to: Andrew Ning (aning@byu.edu)

Abstract. Actuator cylinder theory is an effective approach for analyzing the aerodynamic performance of vertical axis wind turbines at a conceptual design level. Existing actuator cylinder theory can analyze single turbines, but analysis of multiple turbines is often desirable because turbines operate in near proximity within a wind farm. For vertical axis wind turbines, which tend to operate in closer proximity than do horizontal axis turbines, aerodynamic interactions may not be strictly confined to
5   wake interactions. We modified actuator cylinder theory to permit the simultaneous solution of aerodynamic loading for any number of turbines. We also extended the theory to handle thrust coefficients outside of the momentum region, and explicitly defined the additional terms needed for curved or swept blades.

It is found that even out of the wake zone, aerodynamic interactions are not negligible at typical separation distances (i.e., 3–6 rotor diameters). If turbines are co-rotating then for the two turbine cases examined in this paper the sum of the total power
10   was effectively constant except within the wake zone. However, if turbines counter-rotate then both beneficial and detrimental changes in power production were observed depending on the relative positions. However, these benefits are on the order of a few percent and unlikely to be advantageous in practice because of wake interference, except for within highly directional wind sites. Limitations of these analyses identified the need for integration with viscous wake models, and potentially with higher-fidelity induced velocity models.

15   ## 1   Introduction

Blade element momentum theory combines momentum theory across an actuator disk with blade element theory to predict the aerodynamic loading of horizontal axis wind turbines. This theory has been very successful and is heavily used in many analysis and design applications (Hansen, 2008; Manwell et al., 2009; Burton et al., 2011; Ning, 2014). Its primary advantage is computational speed while still providing reasonably accurate performance predictions.

20   Streamtube theory attempts to apply the same concept to vertical axis wind turbine (VAWT) aerodynamic performance estimation (Templin, 1974). Each cross-section of the VAWT (constant height) is approximated as an actuator disk through the mid-plane, which results in a cross-plane actuator line in the 2D plane. However, this model is a rather poor representation of a VAWT as it requires constant flow parameters across the entire disk. An extension of this theory is multiple streamtube theory, where, instead of using one large streamtube passing through the VAWT, the VAWT cross-section is discretized into multiple
25   streamtubes each with an independent induction factor (Wilson and Lissaman, 1974; Strickland, 1975). An additional extension, double multiple streamtube theory (Paraschivoiu, 1981; Paraschivoiu and Delclaux, 1983; Paraschivoiu, 1988), utilizes

two actuator disks to represent the upstream and downstream sides of the cylinder (Fig. 1). In this model momentum losses can occur on both the upwind and downwind faces. Double multiple streamtube theory has been widely used for aerodynamic analysis of VAWTs.
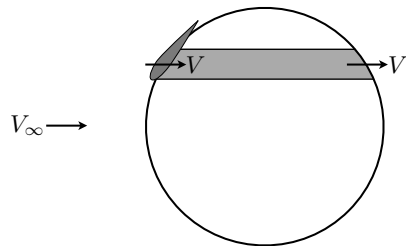
Figure 1. Double multiple streamtube concept with multiple streamtubes along the VAWT (one shown) and separate "actuator disks" on both the upstream and downstream surfaces.

While double multiple streamtube theory is a useful improvement over single streamtube models, it is clearly a forced
5   application of the actuator disk concept to a VAWT. A more physically consistent theory for VAWTs, called actuator cylinder theory, was developed by Madsen (Madsen, 1982; Madsen et al., 2013). Actuator cylinder theory has been shown to be more accurate than double multiple streamtube theory (Ferreira et al., 2014), while still retaining comparable computational speed.

One limitation of actuator cylinder theory is that it is derived only for a single isolated turbine. We are interested in performance of VAWT farms, and thus need to predict performance of multiple VAWTs in proximity to each other. This paper
10   extends the methodology for use with any number of VAWTs, extends applicability to turbines not operating in the momentum region, and adds computation details for blades that are curved or swept. The primary purpose of this paper is to derive the new methodology, but some example trade studies of VAWT pairs are also discussed.

2   Theory Development

The actuator cylinder theory begins with the assumption that a vertical slice of a VAWT can be modeled as a two-dimensional
15   problem. Figure 2 shows a 2D representation of the VAWT, with only one of the blades shown for simplicity, and defines the coordinate system used in this derivation. The VAWT produces a varying normalized radial force per unit length $q(\theta)$ as a function of azimuthal position along the VAWT. We define the positive direction for this force q as positive radial outward (and thus positive radially inward for the loads the fluid produces on the VAWT). Using the two-dimensional, steady, incompressible,
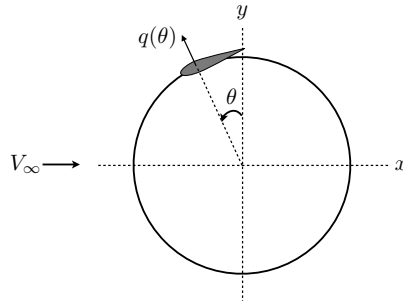
Figure 2. A canonical 2D slice of a VAWT (only one blade shown) and the coordinate system used.

Euler equations, and (for the moment) neglecting nonlinear terms, the induced velocities at any location in the plane can be shown to be given by the following integrals (Madsen et al., 2013; Madsen, 1982):

$$
\begin{aligned}
u(x,y) =& \frac{1}{2\pi} \int_0^{2\pi} q(\theta) \frac{[x+\sin\theta]\sin\theta - [y-\cos\theta]\cos\theta}{[x+\sin\theta]^2 + [y-\cos\theta]^2} d\theta \\
& - q(\cos^{-1} y) \quad \{\text{inside and wake}\} \\
& + q(-\cos^{-1} y) \quad \{\text{wake only}\} \\
v(x,y) =& \frac{1}{2\pi} \int_0^{2\pi} q(\theta) \frac{[x+\sin\theta]\cos\theta + [y-\cos\theta]\sin\theta}{[x+\sin\theta]^2 + [y-\cos\theta]^2} d\theta
\end{aligned}
\tag{1}
$$

where the x,y position is measured from the center of a unit radius turbine, and velocities are normalized by the freestream velocity. For evaluation points inside the cylinder the {inside and wake} term applies, and for evaluation points downstream of the cylinder both the {inside and wake} and {wake only} terms apply. These two terms are based on an integration path through the cylinder, where $\theta = \cos^{-1} y$ (Figure 3). For brevity, the derivation of the above equations are omitted, but details are available in the above cited papers from Madsen.

These two equations for the induced velocities (Eq. (1)) are applicable for any x,y location, however we are primarily interested in the induced velocities only at locations on the current turbine and on other turbines. To facilitate computation we discretize the description of each actuator cylinder into n panels centered at the azimuthal locations:

$$
\begin{aligned}
\theta_i &= (2i-1)\frac{\pi}{n} \quad \text{for } i = 1 \ldots n \\
\Delta\theta &= \frac{2\pi}{n}
\end{aligned}
\tag{2}
$$

Furthermore, as is done in the original version, we assume piecewise constant loading across each panel. These locations are the points of interest where will compute the radial forces and subsequently the induced velocities.
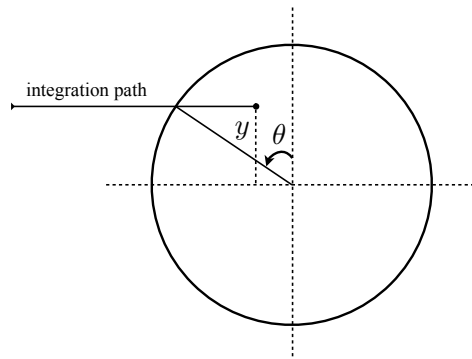
Figure 3. Integration path for a point inside the cylinder.

In general, we need to compute the induced velocity at every location on a given VAWT using contributions from all VAWTs (including itself). In the following derivation we adopt the notation that index I is the turbine we are evaluating the velocities at, and index i represents the azimuthal location on turbine I where we are evaluating. Index J will refer to the turbine producing the induced velocity, and index j will indicate the azimuthal location on turbine J where the load is producing the induced velocity (Fig. 4).
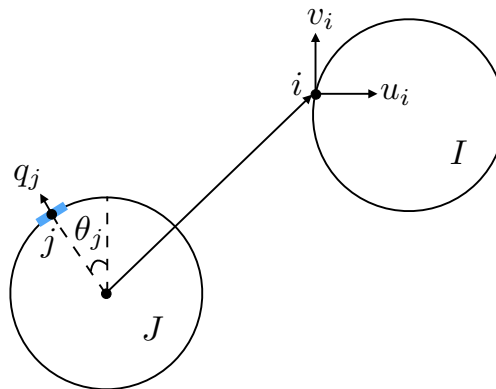
Figure 4. Influence of load at location j of turbine J onto location i of turbine I

Using the azimuthal discretization, the induced velocities at a point (x, y) are expressed as a sum of integrals over individual panels. Recall that Eq. (1) is normalized based on the current VAWT radius and the freestream velocity. Because we are now considering multiple VAWTs with potentially different radii, we need to be more explicit in defining the normalized quantities.

The generalized definitions of the x, y evaluation positions are:

$$x_i^* = (x_i - x_{Jc})/r_J$$
$$y_i^* = (y_i - y_{Jc})/r_J$$

$$(3)$$

where x_{Jc} is the x location of the center of turbine J. If $I = J$ (i.e., we are evaluating the turbine's influence on itself), then this definition is identical to the single turbine case where the x and y locations are then distances from the VAWT center

5   normalized by its radius. The velocity used in normalizing the induced velocities and the radial loading must be the same, and for that purpose we continue to use the freestream velocity. We introduce the star superscript on the induced velocities for clarity (e.g., $u^* = u/V_\infty$). The expressions for induced velocity at the cylinder surface depend on whether we evaluate just upstream of the actuator disk or just downstream. The end result is the same, as long as we are consistent. In the following derivation we evaluate on the upstream surfaces for both halves of the actuator disk.

$$u_i^* = \frac{1}{2\pi} \sum_j q_j \int_{\theta_j - \Delta\theta/2}^{\theta_j + \Delta\theta/2} \frac{(x_i^* + \sin\phi)\sin\phi - (y_i^* - \cos\phi)\cos\phi}{(x_i^* + \sin\phi)^2 + (y_i^* - \cos\phi)^2} d\phi$$

$$- q_{n+1-i} \quad \{I = J, \; i > n/2\}$$

10                $- q_{Jk} + q_{Jn+1-k} \quad \{I \neq J, \; -1 \leq y_i^* \leq 1, \; x_i^* \geq 1\}$ (4)

$$(\text{where index } k \text{ satisfies } \theta_{Jk} = \cos^{-1} y_i^*)$$

$$v_i^* = \frac{1}{2\pi} \sum_j q_j \int_{\theta_j - \Delta\theta/2}^{\theta_j + \Delta\theta/2} \frac{(x_i^* + \sin\phi)\cos\phi + (y_i^* - \cos\phi)\sin\phi}{(x_i^* + \sin\phi)^2 + (y_i^* - \cos\phi)^2} d\phi$$

In these integrals we have replaced θ in the integration with the dummy variable ϕ in order to avoid confusion with the θ terms appearing in the integration limits. The term $-q_{n+1-i}$ arises when evaluating the influence of a turbine on itself. Because we chose to evaluate on the upstream surfaces, the upstream half of the VAWT is considered outside of the VAWT, but the aft half is in the inside of the cylinder. This implies that for the aft half (i.e., $i > n/2$) the $-q(\cos^{-1} y)$ term must be added. This

15   corresponds to the loading on the front half of the turbine with the same y value. Based on our discretization, its location can be indexed directly as $-q_{n+1-i}$.

The following two terms for u arise when turbine I is in the wake of turbine J. Actuator cylinder theory only includes the wake term when an evaluation point is directly downwind from a source point (e.g., the blue region in Fig. 5). The condition corresponds to $x_i^* \geq 1$ and $-1 \leq y_i^* \leq 1$ and $x_i^{*2} + y_i^{*2} \geq 1$. For this wake area, both of the terms in Eq. (1) are applicable. The

20   index k corresponds to the location where $\theta_{Jk} = \cos^{-1} y_i^*$. Note that $\cos^{-1} y_i^*$ will likely not line up exactly with an existing grid point θ_k on turbine J, but we have assumed piecewise constant loading across a given panel, so k will correspond to the panel that is intersected.

This model is based on integration paths like those shown in Fig. 3 and thus ignores the effect of wake expansion and viscous decay. An alternative is to ignore the wake terms and instead apply a momentum deficit factor from some other VAWT wake

model. Because the focus on this paper is on actuator cylinder theory we will use the simple wake model that naturally arises within the theory itself, but this methodology provides a convenient hook to insert any wake model.

Figure 5. Wake region from actuator cylinder theory highlighted in blue (and extending downstream).

For convenience in the computation, Eq. (4) can be expressed as a matrix vector multiplication where the loading q is separated from the influence coefficients.

$$
\begin{aligned}
u_I^* &= A_{x\,IJ}q_J \\
v_I^* &= A_{y\,IJ}q_J
\end{aligned}
\tag{5}
$$

The matrix $A_{y\,IJ}$ is given by:

$$
A_{y\,IJ}(i,j) = \frac{1}{2\pi} \int\limits_{\theta_j - \Delta\theta/2}^{\theta_j + \Delta\theta/2} \frac{(x_i^* + \sin\phi)\cos\phi + (y_i^* - \cos\phi)\sin\phi}{(x_i^* + \sin\phi)^2 + (y_i^* - \cos\phi)^2} d\phi
\tag{6}
$$

For the $A_{x\,IJ}$ matrix we divide the contributions between the direct influence and the wake influence: $A_{x\,IJ} = D_{x\,IJ} + W_{x\,IJ}$ where

$$
D_{x\,IJ}(i,j) = \frac{1}{2\pi} \int\limits_{\theta_j - \Delta\theta/2}^{\theta_j + \Delta\theta/2} \frac{(x_i^* + \sin\phi)\sin\phi - (y_i^* - \cos\phi)\cos\phi}{(x_i^* + \sin\phi)^2 + (y_i^* - \cos\phi)^2} d\phi
\tag{7}
$$

$$
W_{x\,IJ}(i,j) = \begin{cases} -1 & \text{if } -1 \le y_i^* \le 1 \text{ and } x_i^* \ge 0 \\ & \text{and } x_i^{*2} + y_i^{*2} \ge 1 \text{ and } j = k \\ 1 & \text{if } -1 \le y_i^* \le 1 \text{ and } x_i^* \ge 0 \\ & \text{and } x_i^{*2} + y_i^{*2} \ge 1 \text{ and } j = n - k + 1 \\ 0 & \text{otherwise} \end{cases}
\tag{8}
$$

where index k corresponds to the panel where $\theta_{Jk} = \cos^{-1} y_i^*$.

If we are evaluating the influence of a turbine on itself (e.g., $I = J$) then the computations in the A_x matrix can be simplified. We can expand using the definitions for x and y along the cylinder ($x_i^* = -\sin\theta_i$ and $y_i^* = \cos\theta_i$ for $i = 1 \ldots n$). As long as $i \ne j$, then the integral in Eq. (7) evaluates to $\Delta\theta/2$. When $i = j$ the value of the integral depends on which side of the cylinder we evaluate on. It converges to $\pi(-1 + 1/n)$ just outside of the cylinder and $\pi(1 + 1/n)$ just inside. Because we chose to

evaluate on the upstream surface on both halves of the cylinder then the integral evaluates to $\pi(-1+1/n)$ on the upstream half of the cylinder and $\pi(1+1/n)$ on the downstream half of the cylinder.

$$D_{xII}(i,j) = \begin{cases} \Delta\theta/(4\pi) & \text{if } i \neq j \\ (-1+1/n)/2 & \text{if } i = j \text{ and } i \leq n/2 \\ (1+1/n)/2 & \text{if } i = j \text{ and } i > n/2 \end{cases} \qquad (9)$$

$$5 \quad W_{xII}(i,j) = \begin{cases} -1 & \text{if } i > n/2 \text{ and } j = n+1-i \\ 0 & \text{otherwise} \end{cases} \qquad (10)$$

If a user elects to use a more sophisticated wake model the W_x term can simply be ignored and a separate momentum deficit factor can be applied.

2.1 Faster Computation

The bulk of the computational effort is contained in computing the influence coefficient matrices A_{xIJ} and A_{yIJ}. These
10 computations consist of a double loop iterating across all evaluation positions i on turbine I for each source position j on turbine J (which is itself contained in a double loop across all turbines I and J). Fortunately, some of this computation can be simplified. The expressions in Eqs. (6), (9) and (10) apply for the cases where $I = J$, or in other words for computing the influence of the turbine on itself. A significant benefit to this equation form, is that the matrices depend only on the discretization of the cylinder, and not on the details of the blade shape or loading. For a preselected number of azimuthal segments (e.g.,
15 $n = 36$), these matrices can be precomputed and stored. This is true no matter what size radius the VAWT is.

If $I \neq J$ some reduction in computational requirements is also possible. For each VAWT pair ($I \neq J$), if the two VAWTs are of equal radius, then pairs of influence coefficients between them are exactly the same. As seen in Fig. 6, the distance vector from the center of one turbine to the evaluation point on a separate turbine, is exactly equal and opposite to a vector originating from the center of the other turbine and terminating at an azimuthal location diametrically opposite to the first
20 evaluation point's azimuthal location. As long as these two VAWTs are of equal radius, then these two vectors will always be equal and opposite. This corresponds to x^* and y^* switching signs in Eqs. (6) and (7). However, the evaluation locations are always $180°$ apart in location. This corresponds to switching the sign on all sin and cos terms. The two sign changes cancel out and thus the two evaluation coefficients will be exactly the same. In other words, for all pairs of VAWTs that are of equal radii, only one set of influence coefficients need be computed. The influence coefficients for the other VAWT can be mapped
25 over directly. In equation form this is given by

$$D_{xJI}((i+n/2) \bmod n, (j+n/2) \bmod n)$$
$$= D_{xIJ}(i,j), \forall i = 1 \ldots n, j = 1 \ldots n \text{ (if } r_I = r_J) \qquad (11)$$

and similarly for A_y. Note that there is no symmetry in the wake terms (Eq. (8)). If a second turbine is in the wake of the first, the first turbine will clearly not be in the wake of the second turbine.
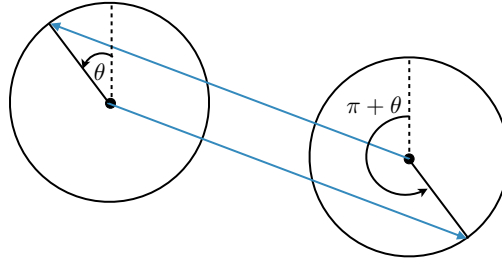
Figure 6. The influence coefficient calculations between a pair of VAWTs will always have paired locations that have exactly equal and opposite distance vectors if the two VAWTs are of equal radius. These two evaluation locations result in the exact same influence coefficients, reducing the amount of calculations that must be performed.

Finally, we can reduce the number of computations required for VAWTs that have large separation distances. If a VAWT pair has a large separation distance (e.g., $\sqrt{(x_{Ic} - x_{Jc})^2 + (y_{Ic} - y_{Jc})^2} > 10 r_I$), then when iterating across index i the value for positions x_i and y_i will change very little. The computation can be simplified by neglecting these very minor changes and instead use the distance between VAWT centers (independent of i):

$$x_i^* \rightarrow (x_{Ic} - x_{Jc})/r_J$$
$$y_i^* \rightarrow (y_{Ic} - y_{Jc})/r_J \tag{12}$$

With this simplification the matrices in Eqs. (6) and (7) can be computing by iterating only in j and filling an entire column per iteration. Additionally, for these large separations the wake terms should be negligible and can be skipped in the computation.

2.2 Body Forces

With the induced velocities u^* and v^*, we can compute the body forces produced by the VAWT. The volume forces produced by the VAWT are modeled as acting along an infinitesimally small radial distance, and in a direction normal to the surface of the cylinder (the tangential component is much smaller than the normal force and can be reasonably neglected in the volume forces of the Euler equations). The radial volume force is

$$f_r(\theta) = \frac{F_r'}{r_j \Delta\theta \Delta r} \frac{L}{\rho V_\infty^2} \tag{13}$$

where F_r' is an azimuthal averaged radial force per unit length in a direction pointing into the center of the cylinder, r_j is the radius of the local VAWT cross-section, and $r_j \Delta\theta \Delta r$ is the in-plane area across which the force acts (Figure 7). The last term comes from the normalization of the Euler equations, where L is some relevant length scale.
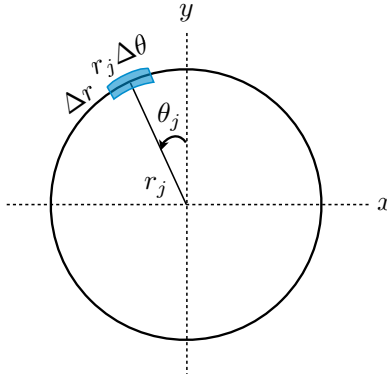
Figure 7. In-plane area for volume force at a given azimuthal station.

Because the force acts across an infinitesimal small radial distance, the radial force acts as a pressure jump

$$
\begin{aligned}
q(\theta) &= \lim_{\epsilon \to 0} \frac{1}{L} \int\limits_{r_j - \epsilon}^{r_j + \epsilon} f_r(\theta)\,dr \\
&= \lim_{\epsilon \to 0} \frac{1}{L} \int\limits_{r_j - \epsilon}^{r_j + \epsilon} \frac{F_r'}{r_j \Delta\theta\,dr} \frac{L}{\rho V_\infty^2}\,dr \\
&= \frac{F_r'}{r_j \Delta\theta} \frac{1}{\rho V_\infty^2}
\end{aligned}
\tag{14}
$$

the $1/L$ is necessary to be consistent with the normalization. It does not matter which reference length is used in normalizing $q(\theta)$ because the length scales cancel.

5 Figure 8 shows the relative components of velocity in the frame of the airfoil. It consists of contributions from the freestream velocity, the velocity due to rotation, and the induced velocities from itself and other turbines.

$$
\boldsymbol{V}_j = V_\infty(1 + u_j)\hat{x} + V_\infty v_j \hat{y} - \Omega_j r_j \hat{t}
\tag{15}
$$

Using the following coordinate transformations

$$
\begin{aligned}
\hat{x} &= -\cos\theta_j \hat{t} - \sin\theta_j \hat{n} \\
\hat{y} &= -\sin\theta_j \hat{t} + \cos\theta_j \hat{n}
\end{aligned}
\tag{16}
$$

10 the velocity can be expressed in the $\hat{n} - \hat{t}$ plane as

$$
\begin{aligned}
\boldsymbol{V}_j =&\, [-V_\infty(1 + u_j)\sin\theta_j + V_\infty v_j \cos\theta_j]\hat{n} \\
&+ [-V_\infty(1 + u_j)\cos\theta_j - V_\infty v_j \sin\theta_j - \Omega_j r_j]\hat{t}
\end{aligned}
\tag{17}
$$
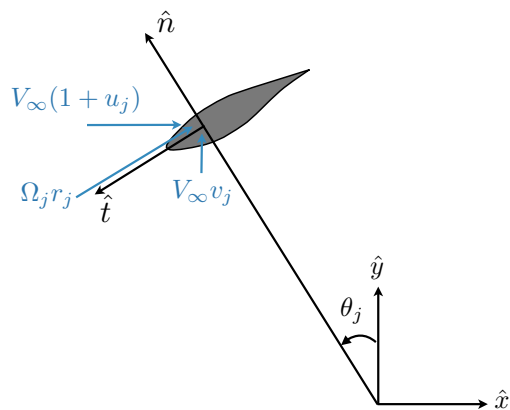
Figure 8. Relative components of velocity in the frame of the airfoil.
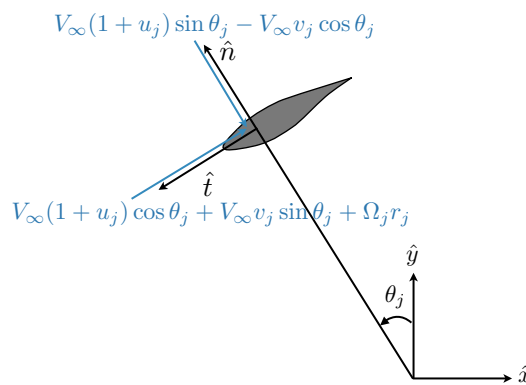
Figure 9. Components of velocity resolved into $\hat{n} - \hat{t}$ plane.

These velocity components are depicted in Figure 9.

If we define the magnitudes

$$V_{nj} \equiv V_\infty (1 + u_j) \sin\theta - V_\infty v_j \cos\theta$$
$$V_{tj} \equiv V_\infty (1 + u_j) \cos\theta + V_\infty v_j \sin\theta + \Omega_j r_j \tag{18}$$

then

5 $$\boldsymbol{V}_j = -V_{nj}\hat{n} - V_{tj}\hat{t} \tag{19}$$

and the magnitude of the local relative velocity and local inflow angle (Fig. 10) are

$$W_j = \sqrt{V_{nj}^2 + V_{tj}^2}$$
$$\phi_j = \tan^{-1}\left(\frac{V_{nj}}{V_{tj}}\right) \tag{20}$$

The angle of attack, Reynolds number, and lift and drag coefficients can then be estimated as

$$\alpha_j = \phi_j - \beta$$
$$Re_j = \frac{\rho W_j c}{\mu}$$
$$c_{lj} = f(\alpha_j, Re_j)$$
$$c_{dj} = f(\alpha_j, Re_j) \tag{21}$$

10 This can be rotated into normal and tangential force coefficients (note that c_n is defined as positive in the opposite direction of $\hat{n}$ in Figure 10).

$$c_{nj} = c_{lj} \cos\phi_j + c_{dj} \sin\phi_j$$
$$c_{tj} = c_{lj} \sin\phi_j - c_{dj} \cos\phi_j \tag{22}$$

We can resolve these normal and tangential loads into a radial, tangential, and vertical coordinate system. In doing so, we will account for blade curvature, as is often used with VAWTs, an example of which is shown in Fig. 11. The total force vector

15 is resolved as

$$F = \frac{1}{2}\rho W^2 (-c_n\hat{n} + c_t\hat{t})\Delta a \tag{23}$$

where the negative sign results from the coordinate system definition seen in Fig. 10. From Fig. 11 we see that the area of the blade element is

$$\Delta a = c\,\Delta s = c\frac{\Delta z}{\cos\delta} \tag{24}$$

20 and the unit vector $\hat{n}$ can be expressed as

$$\hat{n} = \cos\delta\hat{r} + \sin\delta\hat{z} \tag{25}$$
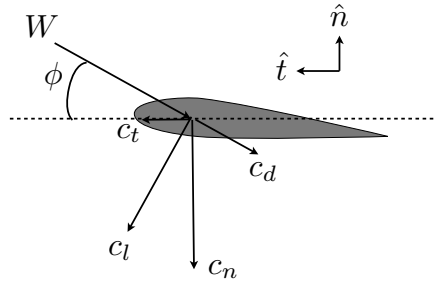
Figure 10. Definition of normal and tangential force coefficients.

Thus, the force vector per unit depth (unit length in the z-direction) is

$$F' = \frac{\rho W^2 c}{2 \cos \delta} (-c_n \cos \delta \, \hat{r} - c_n \sin \delta \, \hat{z} + c_t \, \hat{t}) \tag{26}$$

We can simplify these expressions for the three instantaneous force components

$$R' = -c_n \frac{1}{2} \rho W^2 c$$

$$T' = c_t \frac{1}{2} \rho W^2 \frac{c}{\cos \delta} \tag{27}$$

$$Z' = -c_n \frac{1}{2} \rho W^2 c \tan \delta$$

5   Note that the radial force is unaffected by blade curvature because although the in-plane normal force varies with the cosine of the local curvature angle δ (Fig. 11), the area over which the force acts varies inversely with the cosine of the angle. Blade sweep is also permitted, however it is assumed that the sweep is accomplished through shearing rather than rotation. In other words, it assumed that the airfoils are still defined relative to the streamwise direction as opposed to normal to the local blade sweep. Thus, sweeping does not increase the area of the blade element.

10   For equating with the actuator cylinder theory, only the radial force is of interest (but all components will be of use for computing overall power and loads). Because the blades are rotating we need to compute an azimuthally averaged value of the radial loading (recalling the sign convention for a positive radial loading is inward for loads the fluid produces on the VAWT)

$$F'_{rj} = c_{nj} \frac{1}{2} \rho W_j^2 c \frac{B \Delta \theta}{2\pi} \tag{28}$$

Substituting into Eq. (14) to find that the radial volume force can be expressed as

15    $$q_j = c_{nj} \frac{1}{2} \rho W_j^2 c \frac{B \Delta \theta}{2\pi} \frac{1}{r_j \Delta \theta} \frac{1}{\rho V_\infty^2} \tag{29}$$

After simplification the radial force is

$$q_j = \frac{Bc}{4\pi r_j} c_{nj} \left(\frac{W_j}{V_\infty} \right)^2 \tag{30}$$
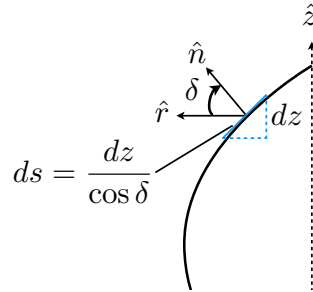
Figure 11. Cross-sectional length of blade segment for small changes in height. Blade curvature increases the area of the blade element for unit height, but sweep has no effect on the blade element area as it is a shearing operation.

Defining solidity as is typically done for a VAWT ($\sigma = Bc/r$) the normalized radial force per unit length becomes

$$q_j = \frac{1}{4\pi}\sigma_j c_{n_j}\left(\frac{W_j}{V_\infty}\right)^2 \tag{31}$$

2.3 Correction Factor

Madsen notes that this linear solution produces good trends for the induced velocities, but is off in magnitude. For a uniform
5 loading across a 2D actuator disk, this linear solution can be shown to produce the following relationship between the thrust coefficient and the induction factor ($a = -u/V_\infty$) (Madsen et al., 2013):

$$C_{T\,linear} = 4\,a_{linear} \tag{32}$$

We can equate this thrust coefficient prediction to that of blade element momentum theory in order to produce a correction factor for a_{linear}. We extend the approach used by Madsen to consider more than just the momentum region. The relationship
10 between the thrust coefficient and the induction factors varies more generally depending on the induction factor (Wilson and Lissaman, 1974; Buhl, 2005)

$$C_T = \begin{cases} 4a(1-a) & a \le 0.4 \text{ (momentum)} \\ \frac{2}{9}(7a^2 - 2a + 4) & 0.4 < a < 1 \text{ (empirical)} \\ 4a(a-1) & a > 1 \text{ (propeller brake)} \end{cases} \tag{33}$$

In order to get the same induction factor from the linear solution, as would be predicted by blade element momentum theory, we need to multiply our predicted induced velocities (and thus the thrust coefficient) by the correction factor $k_a = C_{T\,linear}/C_T$

The correction factors become

$$
k_a = \begin{cases}
1/(1-a) & \text{(momentum)} \\
(18a)/(7a^2 - 2a + 4) & \text{(empirical)} \\
1/(a-1) & \text{(propeller brake)}
\end{cases}
\tag{34}
$$

In order to determine the value of a to use in the above equation we first find the thrust coefficient. The instantaneous thrust coefficient can be found from Eq. (27) using the coordinate system definition that

$$
\begin{aligned}
X' &= -R'\sin\theta - T'\cos\theta \\
&= \frac{1}{2}\rho W^2 c \left(c_n \sin\theta - c_t \frac{\cos\theta}{\cos\delta} \right)
\end{aligned}
\tag{35}
$$

The instantaneous thrust coefficient is

$$
\begin{aligned}
C_{Tinst} &= \frac{X'}{\frac{1}{2}\rho V_\infty^2 (2r)} \\
&= \left(\frac{W}{V_\infty} \right)^2 \frac{c}{2r} \left(c_n \sin\theta - c_t \frac{\cos\theta}{\cos\delta} \right)
\end{aligned}
\tag{36}
$$

where the other normalization dimension comes from the distributed loads, which are a force per unit length in the z-direction. To get the total thrust coefficient we need to compute the azimuthal average

$$
\begin{aligned}
C_T &= \frac{B}{2\pi} \int_0^{2\pi} C_{Tinst}(\theta) d\theta \\
&= \frac{\sigma}{4\pi} \int_0^{2\pi} \left(\frac{W}{V_\infty} \right)^2 \left(c_n \sin\theta - c_t \frac{\cos\theta}{\cos\delta} \right) d\theta
\end{aligned}
\tag{37}
$$

From the thrust coefficient we can compute the expected induction factor by reversing Eq. (33)

$$
a = \begin{cases}
\frac{1}{2}\left(1 - \sqrt{1 - C_T} \right) & C_T \le 0.96 \text{ (momentum)} \\
\frac{1}{7}\left(1 + 3\sqrt{\frac{7}{2}C_T - 3} \right) & 0.96 < C_T < 2 \text{ (empirical)} \\
\frac{1}{2}\left(1 + \sqrt{1 + C_T} \right) & C_T > 2 \text{ (propeller brake)}
\end{cases}
\tag{38}
$$

Finally, this induction factor allows us to compute the correction factor from Eq. (34). These factors should be multiplied against the induced velocities, but because that is the quantity we need to solve for, we must multiply against their predicted values.

Because this correction is derived for an isolated turbine, the correction factors $k_1 \ldots k_N$ should be precomputed for each individual turbine in isolation rather than as part of the coupled solve of all turbines together.

2.4 Matrix Assembly and Solution Procedure

From the proceeding discussion it should be noted that computing that loads depends on the induced velocities, but computing the induced velocities depends on the loads. Thus, an iterative root-finding approach is required. We can assemble the self-induction and mutual induction effects into one large matrix composed of block matrices. We also need to apply the various

5 correction factors k for turbine J. To solve all induced velocities as one large system we will concatenate the u and v velocity vectors into one vector: $w = [u; v]$. In the equation below, the symbol $\odot$ represents an element-by-element multiplication.

$$
\begin{bmatrix} u_1 \\ u_2 \\ \vdots \\ u_N \\ - \\ v_1 \\ v_2 \\ \vdots \\ v_N \end{bmatrix} = \begin{bmatrix} k_1 \\ k_2 \\ \vdots \\ k_N \\ - \\ k_1 \\ k_2 \\ \vdots \\ k_N \end{bmatrix} \odot \begin{bmatrix} A_x & A_{x12} & \dots & A_{x1N} \\ A_{x21} & A_x & \dots & A_{x2N} \\ \vdots & \vdots & \ddots & \vdots \\ A_{xN1} & A_{xN2} & \dots & A_x \\ - & - & - & - \\ A_y & A_{y12} & \dots & A_{y1N} \\ A_{y21} & A_y & \dots & A_{y2N} \\ \vdots & \vdots & \vdots & \vdots \\ A_{yN1} & A_{yN2} & \dots & A_y \end{bmatrix} \begin{bmatrix} q_1 \\ q_2 \\ \vdots \\ q_N \end{bmatrix}
\tag{39}
$$

We now have a matrix vector expression of the form: $w = Aq$, but because q depends on w we must solve for w using a root finding method. The residual equation is:

10 $$f(w) = Aq(w) - w = 0 \tag{40}$$

Any good n-dimensional root finder can be used. This paper uses the modified Powell Hybrid method as contained in hybrd.f of minpack.

2.5 Variations in Height

The actuator cylinder theory computes all loads in 2-dimensional cross-sections. We can either use a representative section to

15 represent the whole turbine (which is more appropriate for an H-Darrieus geometry, ignoring wind shear), or we can additionally discretize the turbine along the height and compute loads at each section.

For each azimuthal station of interest, the solution is projected onto the instantaneous locations of the blade discretization as shown in Fig. 12. For an unswept blade, this involves just a straightforward transfer of forces as the blade discretization would typically be exactly aligned with the surface discretization. However, for swept blades, interpolation is necessary to resolve

20 the forces along the curved blade path. Furthermore, for a swept blade, the normal and tangential directions change along the blade path. For swept blades, each point along the blade is at some azimuthal offset ($\Delta\theta$) from a reference point (e.g., relative to the the equatorial blade location), and the total normal force, tangential force, and torque produced by the blade are (again
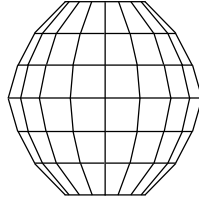
Figure 12. Example two-dimensional discretization in height and azimuthal position of swept surface (side-view).

$\Delta\theta = 0$ for unswept blades)

$$R_{blade}(\theta) = \int [R'(\theta + \Delta\theta)\cos(\Delta\theta)$$
$$- T'(\theta + \Delta\theta)\sin(\Delta\theta)]dz$$
$$T_{blade}(\theta) = \int [R'(\theta + \Delta\theta)\sin(\Delta\theta)$$
$$+ T'(\theta + \Delta\theta)\cos(\Delta\theta)]dz \tag{41}$$
$$Z_{blade}(\theta) = \int Z'(\theta + \Delta\theta)dz$$
$$Q_{blade}(\theta) = \int rT'(\theta + \Delta\theta)dz$$

Now that the forces as a function of θ are known for one blade, the forces for all B blades can be found. We let $\Delta\Theta_j$ represent the offset of blade j relative to the first blade

5 $$\Delta\Theta_j = 2\pi(j-1)/B \tag{42}$$

The resulting forces in the inertial frame are then

$$X_{all-blades}(\theta) = \sum_{j=1}^{B} -R_{blade}(\theta + \Delta\Theta_j)\sin(\theta + \Delta\Theta_j)$$
$$- T_{blade}(\theta + \Delta\Theta_j)\cos(\theta + \Delta\Theta_j)$$
$$Y_{all-blades}(\theta) = \sum_{j=1}^{B} R_{blade}(\theta + \Delta\Theta_j)\cos(\theta + \Delta\Theta_j) \tag{43}$$
$$- T_{blade}(\theta + \Delta\Theta_j)\sin(\theta + \Delta\Theta_j)$$
$$Z_{all-blades}(\theta) = \sum_{j=1}^{B} Z_{blade}(\theta + \Delta\Theta_j)$$

In this representation the velocities at each height can be different to account for wind shear or other wind distributions.

This derivation is provided for completeness, but because of the increased computational expense, and to be consistent with

10 the other comparisons we are making in this paper, we will focus on using one 2D slice for the entire turbine.

2.6 Power

In addition to the thrust coefficient and instantaneous loads, which have already been defined, we are also interested in computing the power coefficient. This is easily computed from the instantaneous tangential load given in Eq. (27) (or Eq. (43)). The torque (per unit length) is then

$$Q = rT' \tag{44}$$

and the azimuthally-averaged power is

$$P = \frac{\Omega B}{2\pi} \int\limits_{0}^{2\pi} Q(\theta)d\theta \tag{45}$$

This is a periodic integral and care should be taken in integrating near the boundaries because of the way the discretization is defined (θ_1 does not start at 0). The power coefficient per unit length is then

$$C_P = \frac{P}{\frac{1}{2}\rho V_\infty^3 (2r)} \tag{46}$$

2.7 Clockwise Rotation

The following derivation assumed counterclockwise rotation. For clockwise rotation a few minor changes must be made. Nothing in the influence coefficients needs changing as those are purely based on location. The only change for clockwise rotation is that the direction of $\hat{t}$ is reversed, as is the direction of the Ωr velocity vector in Figs. 8 and 9. The consequence is

15 that the tangential velocity in Eq. (18) must be redefined as (note the two minus signs)

$$V_{tj} \equiv -V_\infty(1 + u_j)\cos\theta - V_\infty v_j \sin\theta + \Omega_j r_j \tag{47}$$

Additionally, the change in tangential direction affects the computation of the thrust coefficient. In Eq. (35) the sign is reversed on the second part of the equation. The consequence is that the total thrust coefficient (Eq. (37)) would be computed as

$$C_T = \frac{\sigma}{4\pi} \int\limits_{0}^{2\pi} \left(\frac{W}{V_\infty}\right)^2 \left(c_n \sin\theta + c_t \frac{\cos\theta}{\cos\delta}\right) d\theta \tag{48}$$

For transferring loads to an inertial frame, or for computing total blade loads with curved blades, a couple more changes are required. Equation (43) replaces the $+$ sign in front of T_{blade} with a $-$ sign (for both the X and Y equation) and Eq. (41) is modified as:

$$
\begin{aligned}
R_{blade}(\theta) &= \int [R'(\theta + \Delta\theta)\cos(\Delta\theta) \\
&\quad + T'(\theta + \Delta\theta)\sin(\Delta\theta)]dz \\
T_{blade}(\theta) &= \int [-R'(\theta + \Delta\theta)\sin(\Delta\theta) \\
&\quad + T'(\theta + \Delta\theta)\cos(\Delta\theta)]dz
\end{aligned}
\tag{49}
$$

3 Power Variations

This methodology was implemented in Julia and for single turbine cases was validated against Madsen's results (Madsen et al., 2013). Our focus here is on multiple turbine cases, and for simplicity on two turbine cases. We will focus on a scenario with two turbines where turbine 1 is fixed, and a downstream turbine 2 is swept in concentric circles ranging from 1.5 diameters

5 (0.5 radii separation) to 6 diameters between turbine centers (Fig. 13). All turbines are identical, with three NACA 0012 blades and a solidity (Bc/r) of 0.25. The tip-speed ratio for all turbines is kept constant at its optimal isolated value of 3.45 (Fig. 14). Note that the trends reported here can differ significantly at different tip speed ratios, but these conditions are usually of less interests as the turbines are operating suboptimally.
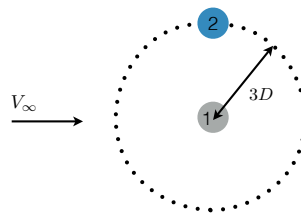
Figure 13. Turbine 1 (gray) is fixed and turbine 2 (blue) is swept out in circles from 1–6 diameters away. This figures shows a swept circle with 3 diameter separation.
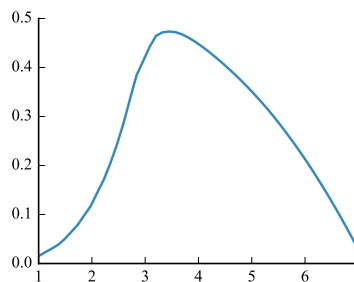
Figure 14. Power coefficient variation versus tip-speed ratio for one VAWT. The optimal tip-speed ratio for this turbine is 3.46.

There are two cases explored here: two turbines co-rotating and two turbines counter-rotating. The left half of Figure 15

10 shows contour plots of normalized power for two co-rotating turbines (rotating counterclockwise when viewed from above): the upper left plot shows the power of the upstream turbine 1 normalized by the power of turbine 1 in isolation ($C_P = 0.473$), the middle left plot shows the power of the downstream turbine 2 normalized in the same manner, and the bottom left plot shows the combined power of the two turbines normalized by their combined power in isolation.

We see in the top two figures that significant interference occurs between the turbines. Even at 6 diameters spacing, the power deviates from the isolated power by up to 3%. When turbine 2 is downstream, but outside of the wake, the power of turbine 1 is less than the isolated power, while the power of turbine 2 is higher than the isolated power.

However, if we look at the combined power produced by turbine 1 and 2 (bottom left of Fig. 15) we note that the positive
5   and negative interference effectively cancel out. The total power of the two turbines is essentially equal to their total power in isolation, except, of course, in the wake region.
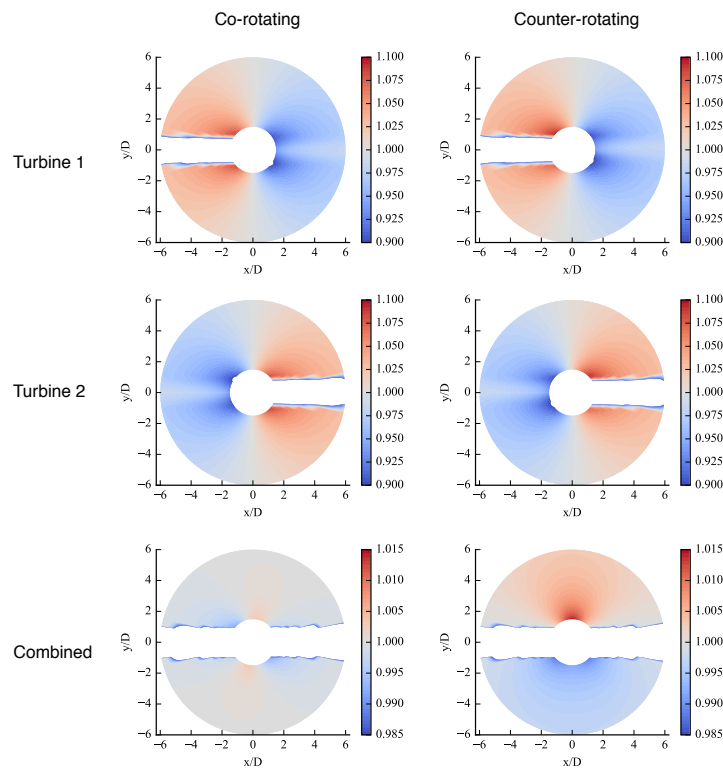
Figure 15. Power contours for a pair of co- and counter-rotating turbines normalized by the the power of the turbine(s) operating in isolation. For the combined case the normalization is with respect to the total isolated power of both turbines. Turbine 1 is fixed at (0, 0) and the downstream turbine 2 is moved. The reported power occurs when turbine 2 is at the given location. Wind direction is from left to right, and distance is measured between turbine centers.

The same analysis is repeated, but for counter-rotating turbines (right half of Fig. 15). In this case turbine 1 is rotating counterclockwise, and turbine 2 is rotating clockwise when viewed from above. Note that the differences are subtle for the individual powers as compared to the co-rotating case, but the combined power of the turbines is notably different. In the

co-rotating case, the locations of power increase of turbine 2 are highly correlated with locations of power decrease for turbine 1, meaning that they mostly cancel out. However, in the counter-rotating case, the locations of maximum benefit and maximum detriment occur on opposite sides. The result is that there is a half plane with small power increases, and a half plane with small power decreases, both with a change in power of about 1% or less at reasonable separation distances.

5 The configuration with positive interference (as predicted by this method, and at this tip-speed ratio) is the Counter Up case shown in Fig. 16. To understand why, one needs to examine the torque distributions and the induced velocity field. The torque distributions for an isolated clockwise and counterclockwise turbine are shown in Fig. 17.
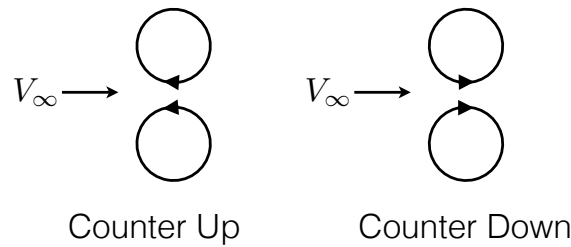
Figure 16. Two cases for a counter rotating pair of turbines. "Counter Up" refers to the pair with a rotation direction facing upstream at their closest interface, where as the "Counter Down" configuration rotates downstream at their closest interface. Actuator cylinder theory predicts a positive interference for the Counter Up configuration when operating at the optimal tip-speed ratio.
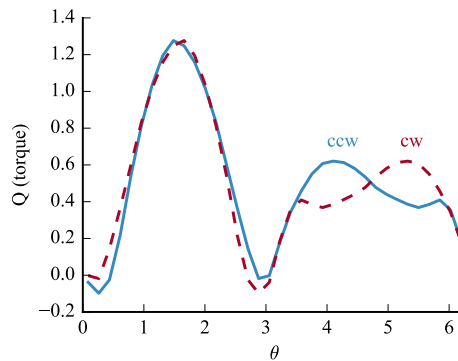
Figure 17. Torque distribution for a clockwise and counterclockwise rotating turbine (both in isolation).

For a VAWT, whether rotating clockwise or counterclockwise, the azimuthal location of largest power production is at $\theta = 90°$ (see Fig. 18). The rotation velocity is always in the tangential direction, but at $90°$ the freestream velocity is perpendicular 10 to the tangential direction thereby generating the largest force in the tangential direction (and thus the largest torque). To most

effectively increase toruqe through mutual induction, the induced velocity should be perpendicular to the direction of the airfoil motion, in this case in the freestream direction.

The azimuthal location of next largest power production depends on whether the VAWT is rotating clockwise or counter-clockwise. But in all cases, the most beneficial induced velocities (in terms of producing power) should be perpendicular to the tangential motion of the airfoil as shown in Fig. 19.
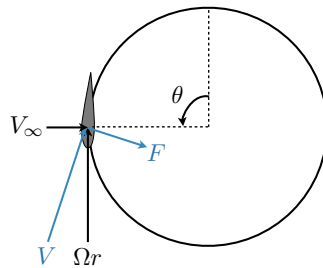
Figure 18. Location of maximum power generation on a VAWT. V is the total velocity vector, and the generated force F is always perpendicular to V.

CCW   CW
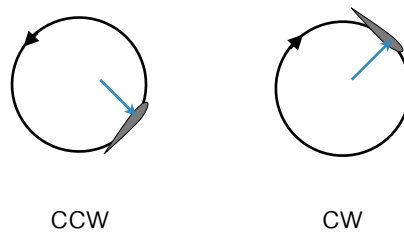
Figure 19. Location of second highest power production depending on whether turbine is rotating clockwise or counter-clockwise. The blue arrow indicates the direction of induced velocity that would created the largest torque (and thus power).

The streamlines for the induced velocity field of the isolated VAWT and the total velocity field (with freestream added) are shown in Fig. 20. This velocity field is not an artifact of removing the nonlinear terms in the Euler equations. The streamlines for a solution of an actuator cylinder based on the full Euler equations yields essentially the same induced and total velocity fields (see Figs. 10 and 11 on pg. 66 of (Madsen, 1982)), as does an unsteady panel simulation of a VAWT (see Figs. 3.7 and 3.8 in (Ferreira, 2009)).

From this induced velocity field we can understand why the power production changes as observed in the previous contour plots. On the upwind half of the domain there is an induced velocity in the upstream direction. This reduces the effective angle of attack at the location of maximum power production (Fig. 18), and thus reduces the produced power. For the secondary peak locations (Fig. 19) we see that the best configuration will place the clockwise rotating turbine above the counterclockwise

rotating turbine so as to create an induced velocity field that is mutually beneficial. The Counter Up configuration (Fig. 16) is indeed the one that is observed to be mutually beneficial in these simulation. Figure 21 shows the torque distribution for the counterclockwise turbine both isolated and in a paired Counter Up configuration (Fig. 16). The power increase on the downstream half is larger than the power decrease on the upstream half leading to an overall power increase. Conversely, the

5   Counter Down configuration experiences a decrease in power on both the upwind an downwind portions of the VAWT. Note that this case focuses on turbines operating near their optimal tip-speed ratio, but the relative benefits and interference change with different tip-speed ratio.
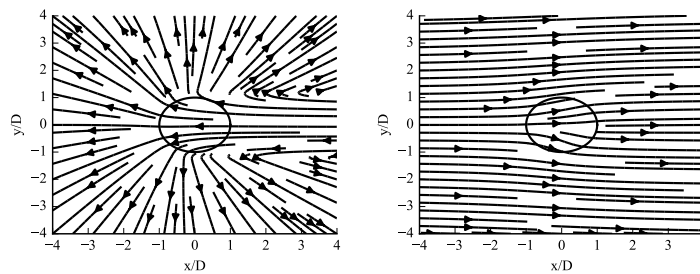
Figure 20. Streamlines for an isolated turbine. The left figure shows the induced velocity only, while the right figure includes the freestream.
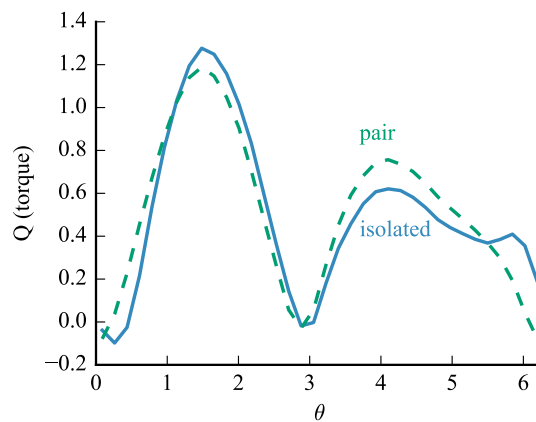
Figure 21. A counterclockwise turbine operating in isolation and in a co-rotating pair according ot Fig. 16.

Results of higher fidelity simulations and experiments of counter-rotating turbines show mixed results. An unsteady RANS simulation of two VAWTs in the Counter Down configuration, rotating out of phase, shows a small decrease in power (Ko-

10   robenko et al., 2013), consistent with that observed here. However, another unsteady RANS simulation shows positive benefits

for both co-rotating and counter-rotating pairs of turbines (Bremseth and Duraisamy, 2016) (although it should be noted that their reported power coefficients are unrealistically high, even for the isolated turbine). The difference is that their simulations predict an positive (downwind) induced velocity on the upper half of the turbines, opposite to that observed in the previously mentioned studies. In that case the upwind half of the turbine experiences an increase in power. Using this actuator cylinder

5 theory, but forcing the induced velocity on the upwind half of the turbine to be in the positive downwind direction, we also observe positive interference for co-rotating and both counter-rotating configurations consistent with these published results.

We can also compare these results to experimental data. An experimental database of VAWT arrays arranged in different configurations was collected over an approximately two year period by The Caltech Field Laboratory for Optimized Wind Energy[1]. From this dataset we extract three cases: an isolated turbine, a Counter Up pair, and a Counter Down pair (Fig. 16).

10 The full wind farm dataset is filtered so that only configurations with one pair in the first row of an array are considered to eliminate wake effects and side array effects, only inflow angles within $10°$ of a perpendicular inflow angle are used, and only freestream velocities within half a standard deviation of the optimal tip-speed ratio for that turbine ($\lambda^* = 2.3$) are used to best match the conditions of our simulations (standard deviations in wind speed are contained in the experimental data).

A box plot of the power coefficients for the three configurations are shown in Fig. 22. On average the Counter Down

15 configuration shows a benefit over the isolated turbine, whereas the Counter Up configuration shows a decrease in power. However, the variation in the data is large enough that the differences are not statistically significant.
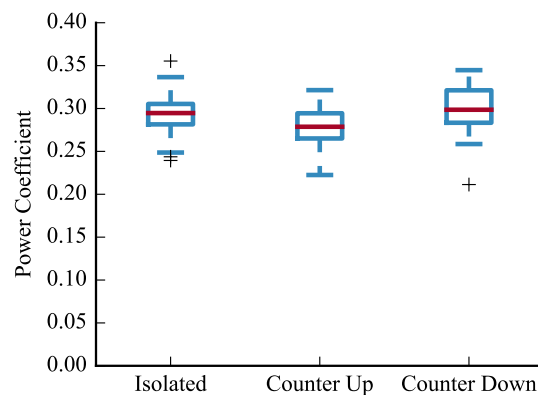
Figure 22. Boxplot comparing the power coefficient of three configurations. The red center line denotes the median, and the top and bottom of the box denote the 25% and 75% quartiles. The whiskers extend to show the range of the data with the + symbols indicating outliers.

---

[1] http://flowe.caltech.edu

4   Conclusions

Actuator cylinder theory is a fast and effective analysis method to predict aerodynamic loads and power of vertical axis wind turbines. In this paper we derive an extension to actuator cylinder theory for multiple interacting turbines. Additional extensions were provided that apply to both the single turbine and multiple turbine cases: thrust coefficients outside of the momentum regions, and curved or swept blades. Analysis of pairs of turbines found that for co-rotating turbines the increases and decreases in power production mostly cancelled out, whereas for counter-rotating pairs positive or negative power benefits were observed.

Analysis with multiple turbines highlighted the need for model improvements in the wake region and in the induced velocity fields. First, an improved wake model is necessary because the wakes in actuator cylinder theory are inviscid, do not decay, and do not spread. Our recent work has developed the first VAWT wake model derived from computational fluid dynamics simulations that is parametrized for turbines with different tip-speed ratios and solidities (Tingey and Ning, 2016). Models like this could be combined with actuator cylinder theory to better predict turbine-wake interactions.

Second, the induced velocity field predicted in this method, while consistent with other published inviscid induced velocity fields, may not be accurate as compared to real turbulent, viscous flow. We observed that conclusions on increases or decreases in power from counter-rotating turbines are sensitive to the accuracy of this induced velocity field and that mixed scenarios have been reported in the literature. These induced velocities may depend on the relative phase of the rotating turbines.

The potential benefits of mutual induction from close spacing are much less important than the wake effect. In previous published studies the power increase from mutual induction is on the order of a few percent. However, all of these studies, both numerical and experimental (Bremseth and Duraisamy, 2016; Korobenko et al., 2013; Araya et al., 2014), either use a freestream wind from a single direction or a site with a highly directional wind rose. For sites with larger variations in wind directions (which is most sites), any beneficial effects from close placement would be negated by wake effects when considering the expected value of the power across the full wind rose. Our past research in HAWT wind farm optimization suggests that when optimizing turbine positioning, under uncertainty of wind direction, optimal configurations are spread out and not in aligned rows (Fleming et al., 2016; Gebraad et al., 2015). For VAWTs, a tighter spacing may be possible than for HAWTs, as VAWTs tend towards lower optimal tip-speed ratios which produces shorter wakes. However, a tighter spacing does not necessarily mean better performance than a HAWT farm. Power density is generally a poor metric for comparing performance, and future studies with a cost of energy analysis are needed to draw conclusions on optimal configurations and spacings of VAWT wind farms.

If the mutual induction is augmented with a separate model, or is deemed less important because of a fuller wind rose, than the single actuator cylinder theory with a separate wake model is likely the best approach for speed and accuracy. Regardless, of which approach is used, the extensions shown in this paper for regions outside of the momentum region and for curved and swept blades are useful in all cases. All code developed for this analysis has been made open source and is freely available online[2].

---

[2]http://flow.byu.edu/publications/

References

Araya, D. B., Craig, A. E., Kinzel, M., and Dabiri, J. O.: Low-order modeling of wind farm aerodynamics using leaky Rankine bodies, J. Renewable Sustainable Energy, 6, 063 118, doi:10.1063/1.4905127, http://dx.doi.org/10.1063/1.4905127, 2014.

Bremseth, J. and Duraisamy, K.: Computational analysis of vertical axis wind turbine arrays, Theor. Comput. Fluid Dyn., doi:10.1007/s00162-016-0384-y, http://dx.doi.org/10.1007/s00162-016-0384-y, 2016.

Buhl, M. L.: A New Empirical Relationship between Thrust Coefficient and Induction Factor for the Turbulent Windmill State, Tech. Rep. NREL/TP-500-36834, National Renewable Energy Laboratory, 2005.

Burton, T., Jenkins, N., Sharpe, D., and Bossanyi, E.: Wind Energy Handbook, Wiley, 2nd edn., 2011.

Ferreira, C. S.: The Near Wake of the Vawt, Ph.D. thesis, Delft University of Technology, 2009.

Ferreira, C. S., Madsen, H. A., Barone, M., Roscher, B., Deglaire, P., and Arduin, I.: Comparison of Aerodynamic Models for Vertical Axis Wind Turbines, J. Phys.: Conf. Ser., 524, 012 125, doi:10.1088/1742-6596/524/1/012125, http://dx.doi.org/10.1088/1742-6596/524/1/012125, 2014.

Fleming, P., Ning, A., Gebraad, P., and Dykes, K.: Wind Plant System Engineering through Optimization of Layout and Yaw Control, Wind Energy, 19, 329–344, doi:10.1002/we.1836, 2016.

Gebraad, P., Thomas, J. J., Ning, A., Fleming, P., and Dykes, K.: Maximization of the Annual Energy Production of Wind Power Plants by Optimization of Layout and Yaw-Based Wake Control, Wind Energy, (accepted), 2015.

Hansen, M. O. L.: Aerodynamics of Wind Turbines, Earthscan, 2nd edn., 2008.

Korobenko, A., Hsu, M.-C., Akkerman, I., and Bazilevs, Y.: Aerodynamic Simulation of Vertical-Axis Wind Turbines, Journal of Applied Mechanics, 81, 021 011, doi:10.1115/1.4024415, http://dx.doi.org/10.1115/1.4024415, 2013.

Madsen, H.: The Actuator Cylinder — a Flow Model for Vertical Axis Wind Turbines, Ph.D. thesis, Aalborg University Centre, 1982.

Madsen, H., Larsen, T., Vita, L., and Paulsen, U.: Implementation of the Actuator Cylinder Flow Model in the HAWC2 Code for Aeroelastic Simulations on Vertical Axis Wind Turbines, in: 51st AIAA Aerospace Sciences Meeting, AIAA 2013-0913, doi:10.2514/6.2013-913, 2013.

Manwell, J. F., Mcgowan, J. G., and Rogers, A. L.: Wind Energy Explained, Wiley, 2nd edn., 2009.

Ning, A.: A Simple Solution Method for the Blade Element Momentum Equations with Guaranteed Convergence, Wind Energy, 17, 1327–1345, doi:10.1002/we.1636, http://dx.doi.org/10.1002/we.1636, 2014.

Paraschivoiu, I.: Double Multiple Streamtube Model for Darrieus Wind Turbines, in: 2nd DOE/NASA Wind Turbine Dynamics Workshop, Cleveland, OH, 1981.

Paraschivoiu, I.: Double-multiple streamtube model for studying vertical-axis wind turbines, Journal of Propulsion and Power, 4, 370–377, doi:10.2514/3.23076, http://dx.doi.org/10.2514/3.23076, 1988.

Paraschivoiu, I. and Delclaux, F.: Double Multiple Streamtube Model with Recent Improvements (for Predicting Aerodynamic Loads and Performance of Darrieus Vertical Axis Wind Turbines), Journal of Energy, 7, 250–255, doi:10.2514/3.48077, 1983.

Strickland, J.: A performance prediction model for the Darrieus turbine, in: International Symposium on Wind Energy Systems, vol. 1, p. 3, 1975.

Templin, R.: Aerodynamic performance theory for the NRC vertical-axis wind turbine, LTR-LA-160, National Aeronautical Establishment, Ottawa, Ontario, Canada, 1974.

Tingey, E. and Ning, A.: Parameterized Vertical-Axis Wind Turbine Wake Model Using CFD Vorticity Data, in: ASME Wind Energy Symposium (AIAA SciTech), San Diego, CA, doi:10.2514/6.2016-1730, 2016.

Wilson, R. and Lissaman, P.: Applied Aerodynamics of Wind Power Machines, Tech. rep., Oregon State University, 1974.